Ionics (2015) 21:1857–1866
DOI 10.1007/s11581-015-1366-6

ORIGINAL PAPER

Influence of carbon content, particle size, and partial manganese substitution on the electrochemical performance of $LiFe_xMn_{1-x}PO_4$/carbon composites

N. A. Hamid · S. Wennig · A. Heinzel · C. Schulz · H. Wiggers

Received: 18 August 2014 / Revised: 12 December 2014 / Accepted: 6 January 2015 / Published online: 24 January 2015

Abstract $LiFePO_4$/C and $LiFe_xMn_{1-x}PO_4$/C (x=0.7) nanocomposites were successfully synthesized via scalable spray-flame synthesis followed by solid-state reaction. A solution of iron (III) acetylacetonate and tributyl phosphate in toluene was used to produce amorphous, nanosized $FePO_4 \cdot H_2O$ in a spray-flame reactor which was then milled with Li_2CO_3 and glucose to produce a $LiFePO_4$/C composite material in a solid-state reaction. The influence of calcination temperature and carbon content on the properties of the resulting material was investigated using specific surface area measurements (BET), X-ray diffraction (XRD), electron microscopy, and electrochemical characterization. The impact of manganese addition on the electrochemical behavior was analyzed using cyclic voltammetry (CV) and constant-current (CC) measurements. XRD shows that the combination of gas-phase synthesis and subsequent solid-state reaction yields highly pure $LiFePO_4$/C. BET measurement revealed that the particle size of $LiFePO_4$ in the composite depends on the amount of glucose. A discharge capacity of more than 140 mAh/g at C/20 is achieved for $LiFePO_4$/C with a carbon content of 6 wt%. This material supports high charge as well as discharge rates delivering more than 60 mAh/g at 16 C and sustains good cycle stability providing 115 mAh/g at 1 C. The energy density of the olivine increases about 10 % by substituting 30 mol% of iron by manganese while preserving the electrochemical performance of pure $LiFePO_4$/C.

Keywords Nano $FePO_4$ · $LiFePO_4$/C · Doped $LiFePO_4$/C · Li-ion batteries · Electrochemical properties · Spray-flame synthesis

N. A. Hamid · C. Schulz · H. Wiggers
Institute for Combustion and Gas Dynamics—Reactive Fluids (IVG), University of Duisburg-Essen, Duisburg, Germany

S. Wennig · A. Heinzel
The Fuel Cell Research Center ZBT, Duisburg, Germany

A. Heinzel · C. Schulz · H. Wiggers
Center for Nanointegration Duisburg-Essen, CENIDE, Essen, Germany

H. Wiggers (✉)
University of Duisburg-Essen, Carl-Benz-Str. 199, 47057 Duisburg, Germany
e-mail: hartmut.wiggers@uni-due.de

Introduction

The widespread use of lithium ion batteries causes continuous efforts in the development of low-cost high-performance materials. Alternative cathode materials for the expensive and noxious cobalt- and nickel-based oxides that are currently used in commercial lithium ion batteries are of high interest. Some of the most promising candidates are olivines $LiMPO_4$ with (M=Mn, Fe) due to high availability of the required raw materials and low material costs. They typically show flat voltage profiles and are environmentally benign compared to the state of the art materials such as $LiCoO_2$ [2]. However, in contrast to the conventional materials, olivines exhibit poor electronic conductivity and low ionic diffusivity leading to a limited high-rate performance [7]. There are strategies to overcome these limitations, for instance by coating of the active material with conductive carbon [4, 5, 11, 16, 23, 26], utilization of nanostructured particles [17, 33, 35], and doping with bivalent cations such as Mg, Ni, and Co [32]. The combination of carbon coating and nanostructuring enhances the electronic as well as the ionic conductivity, and the resulting electrochemical performance makes these materials highly promising for high-power applications [21]. An intimate connection between carbon and the olivine in a stable

nanocomposite is indispensable, because carbon significantly facilitates the electron transport. Thus, the electrical conductivity of the active material is increased, which in turn offers excellent electrochemical performance [15]. Moreover, the presence of carbon during the solid-state reaction ensures reducing conditions leading to a preferential formation of the desired Fe^{2+} species. It is also known that carbon suppresses the grain growth of olivine during the annealing process, thus maintaining small particles sizes [31].

Various methods with respect to the synthesis of $LiFePO_4$ were developed and optimized to meet the requirements for current applications. An improvement of the intrinsic conductivity of $LiFePO_4$ by coating with 6.8 wt% of carbon using a solid-state reaction was reported by Zhang et al. resulting in a material that delivers 144 mAh/g at 1 C [37]. With the same method, Mi et al. reported about the synthesis of $LiFePO_4$ with a particle size distribution between 200 and 500 nm and 3.7 wt% of carbon providing 118 mAh/g at 1 C [26]. $LiFePO_4$ with a 3 to 5 nm thick carbon coating prepared by a sol–gel method offers a discharge capacity of 112 mAh/g at 0.1 C [17]. Another promising route is the mechanical activation of olivine reported by Kim et al. who demonstrated that 100 nm size $LiFePO_4$/C is capable to deliver 140 mAh/g at a 1 C rate [1]. To summarize, a multitude of parameter such as annealing temperature and amount as well as thickness of carbon must be taken into consideration while synthesizing $LiFePO_4$ as these criteria can dramatically affect the electrochemical performance. With respect to the solid-state reaction, it must be considered that temperatures above 800 °C lead to the formation of additional phases such as Fe_2P, Fe_2O_3, and $Li_3Fe_2(PO_4)_3$. In contrast, the reaction at temperatures below 500 °C lacks of incomplete reduction of Fe^{3+}, which could be detected by Mößbauer experiments [20]. Therefore, heating between 600 and 700 °C is known to provide well-crystallized and high-purity samples [31]. In addition, the electrochemical performance of $LiFePO_4$/C heavily relies on the quantity as well as the quality of conductive carbon used for improved conductivity.

We investigated the formation of nanocomposite $LiFePO_4$/C in a two-stage process. Iron phosphate nanoparticles are produced in a spray-flame synthesis reactor from iron (III) acetylacetonate and tributyl phosphate dissolved in toluene, a method that is known to be scalable in production capacity [28]. Nanocomposite $LiFePO_4$/C is produced from iron phosphate nanoparticles, lithium carbonate, and glucose in a subsequent high-temperature solid-state reaction. The influence of reaction temperature and glucose content was investigated to optimize the electrochemical properties of the resulting nanocomposite. Additionally, 30 mol% of the iron precursor was substituted by manganese acetylacetonate to produce $Fe_{0.7}Mn_{0.3}PO_4$. Due to the higher redox potential of Mn^{2+}/Mn^{3+} compared to Fe^{2+}/Fe^{3+}, the energy density of $LiFe_xMn_{1-x}PO_4$ should be higher than that of pure $LiFePO_4$, which is beneficial for high-power as well as high-energy applications [22, 30, 34].

Materials and methods

Materials synthesis

Nanoscale $FePO_4{\cdot}x\ H_2O$ and $Fe_{0.7}Mn_{0.3}PO_4{\cdot}xH_2O$ were produced in the gas phase by spray-flame synthesis. Liquid precursor solutions composed of 0.35 mol/l iron (III) acetylacetonate ($Fe(acac)_3$) and 0.35 mol/l tributyl phosphate (reagent grade, Merck) dissolved in toluene (reagent grade, Merck) were prepared. In case of the mixed iron/manganese phosphate, 30 mol% of $Fe(acac)_3$ was replaced by manganese (III) acetylacetonate. The precursor solutions were injected into a spray-flame synthesis reactor at a constant flow rate of 3 ml/min and atomized by means of a coaxial dispersion gas flow of 5 slm O_2. The resulting spray was ignited by a premixed methane/oxygen flame. The flame was stabilized with a coaxial sheath gas flow of 5 slm O_2. Details of the synthesis are described elsewhere [12].

The $LiFePO_4$/C and $LiFe_xMn_{1-x}PO_4$/C composite materials were synthesized from the as-prepared phosphates. Li_2CO_3 (reagent grade, Merck) and various amounts of glucose, which acts as reducing agent and carbon source simultaneously, were mixed with analytical grade ethanol and the respective phosphates. Milling of the mixtures was conducted for 12 h using a Netzsch Labstar LS1 with 0.5 mm zirconia beads and zirconia vial. After drying and preheating of the milled dispersion at 80 °C for 24 h, the obtained powder mixture was pelletized at 15 kN and calcined under nitrogen at various temperatures in the 600 to 800 °C range. Gray-colored products were obtained after cooling down to room temperature. The gray becomes darker with increasing glucose content. Prior to electrode preparation, the materials were ground and dry sieved on an electric shaker to determine the size fraction <25 μm.

Materials characterization

The phase composition of all products was determined by X-Ray diffraction (XRD) performed with a PANalytical X-ray diffractometer (X'Pert PRO) with Cu K_α radiation (1.5406 Å). The specific surface area (SSA) determined via nitrogen adsorption (Brunauer-Emmet-Teller, Quantachrome Nova 2000) was used to calculate equivalent particle diameters assuming spherical shape with the density of bulk olivine by using the following equation

$$d/\mathrm{nm} = 10^6 \frac{6}{\rho \mathrm{SSA}}, \quad (1)$$

where ρ is the density of $LiFePO_4$ in kilogram per cubic meter. The change in density for the carbon-coated particles was

considered with respect to the carbon mass content. The morphology of the materials was investigated by transmission electron microscopy (TEM, Philips CM12) operated at an acceleration voltage of 120 kV. The carbon content of the $LiFePO_4$/C composite was determined by an element analyzer (CE instruments EA1110). Raman spectroscopy was performed with a micro-Raman system using a wavelength of 532 nm and a liquid-nitrogen cooled CCD to analyze the relation between sp^2 and sp^3carbon. Electrical characterization of the pristine particles was carried out by impedance spectroscopy. Samples of the nanoparticles were prepared by uniaxial pressing 30 mg of the powder into thin coplanar disks of 5 mm diameter at a force of 1.02 GPa for 30 min. The thickness of the disks was measured and the compressed disks were sandwiched between two 5 mm platinum electrodes and mounted in a measurement cell, see [13]. Impedance measurements were performed with a Solartron 1255 impedance spectrometer in the frequency range between 1 Hz and 1 MHz with 20 frequency points per decade and specific conductivities were obtained from the low-frequency fit of the sample resistances and the geometry of the measurement setup.

Electrode preparation

$LiFe_xMn_{1-x}PO_4$/C (x=0.7 and 1, respectively) and Super-P Li™ (Timcal) were intensely mixed in a mortar, subsequently dispersed by sonication for 2 min and homogenized with a turbo mixer at 10,000 rpm for 60 min in a solvent composed of analytical grade ethanol, ultrapure water, and polyacrylic acid (PAA, Alfa Aesar®, 25 wt% solution in water, average M_w: 240,000 g/mol). The obtained slurry was cast on an aluminum foil (Alujet, thickness 30 μm) with a wet film thickness of 100 μm by using an adjustable doctor blade and dried under vacuum at 90 °C. The samples were cut into electrodes with an area of 1.1 cm^2. The typical composition of the dried electrode material was 88 wt% $LiFe_xMn_{1-x}PO_4$/C, 7 wt% Super-P Li™, and 5 wt% PAA.

Electrochemical measurements

Electrochemical measurements were carried out using Swagelok-type electrode cells. The test cells were assembled in an argon-filled glove box. Lithium foil (Rockwood Lithium, 100 μm thick) served as counter and reference electrode and polypropylene fleeces impregnated with the electrolyte were used as separator. For investigations with respect to the carbon content, a solution of 1 M $LiPF_6$ in ethylene carbonate (EC) and diethyl carbonate (DEC) (30 %/70 % by mass) was used as electrolyte. Constant-current (CC) and cyclic-voltammetry (CV) measurements were performed with a Basytec CTS Lab XL battery tester. CC experiments were carried out in the range of 2.6 to 4.2 V versus Li/Li^+. CVs were recorded with a scan rate of 10 μV/s between 2.6 and 4.2 V versus Li/Li^+.

For the analysis of manganese-containing $LiFe_xMn_{1-x}PO_4$/C, a solution of 1 M $LiPF_6$ in EC and dimethyl carbonate (DMC) (50 %/50 % by mass) was used due to its higher electrochemical stability compared to EC/DEC. CC and CV measurements were performed with the equipment mentioned above. CC experiments were carried out in the range of 2.6 to 4.7 V versus Li/Li^+, and CVs were recorded with a scan rate of 10 μV/s between 2.6 and 4.9 V versus $Li/Li^+$for Mn doped $LiFePO_4$/C.

Results and discussion

$LiFePO_4$/C with various carbon contents

As the formation of $LiFePO_4$ (olivine) from nanoscale $FePO_4 \cdot x H_2O$ starts at 600 °C [12], we investigated the formation of olivine in the 600 to 800 °C range with 50 K increments. Figure 1 shows the XRD results of the respective materials.

The crystal size of the as-received materials was determined from the x-ray diffraction patterns by Rietveld refinement using MAUD [25]. The particle size increases from 34 (600 °C) to 48 nm (800 °C). This trend was also observed for $LiFePO_4$/C synthesized by spray-flame synthesis [10, 19], in solid-state reactions [4, 8], or sol–gel synthesis [23]. From Fig. 1, it is obvious that an increasing amount of Fe_2P is formed from 700 °C while some traces of FeP arise at lower temperature. Though contributions of Fe_2P—in contrast to FeP—are beneficial for enhancing the electronic conductivity, major amounts deteriorate the electrochemical performance due to reduction of electrochemically active

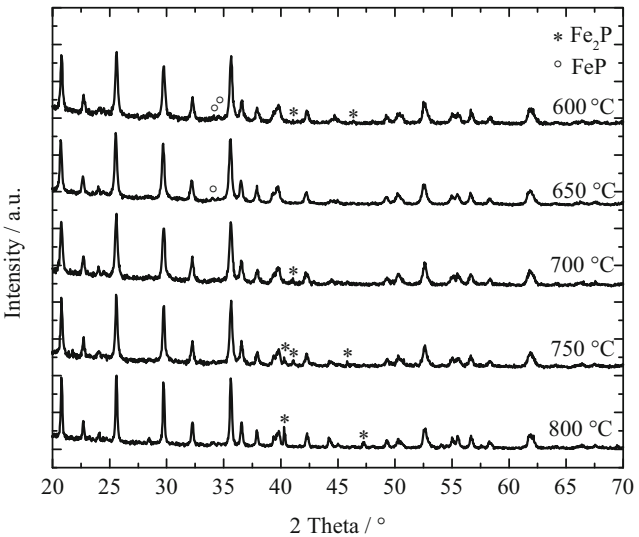

Fig. 1 XRD patterns of $LiFePO_4$/C prepared by solid-state synthesis at various temperatures. Signals originating from Fe_2P and FeP are marked by a *star* and a *circle*, respectively

material [19, 23] and therefore both should be avoided. To sum up, we suggest a heating temperature of 700 °C.

The residual carbon content determined by elementary analysis was found to decrease gradually from 5.8 (600 °C) to 2 wt% (800 °C) when applying an initial glucose content of 20 wt%. This shows that increasingly more carbon is consumed at higher temperature.

The influence of glucose amount on composition and resulting carbon content was investigated for mixtures in the 10 to 30 % range with 5 % increments. Figure 2 shows X-ray diffraction diagrams of the respective $LiFePO_4$/C composites synthesized at 700 °C. The diffraction patterns agree well with the expectations for orthorhombic olivine (JCPDS card number: 40-1499) and no additional phases were observed. Mößbauer and XPS spectroscopy (not shown) revealed that the oxidation state of iron is mostly Fe^{2+} as required with a slight oxidation at the surface resulting in some Fe^{3+}. While the signal intensity decreases indicating a decreasing crystallinity, the amount of residual carbon increases from 2.1 to 7.3 wt% for mixtures with 10 and 30 wt% glucose, respectively. The resulting materials properties are given in Table 1.

The results confirm that higher carbon contents increasingly hinder particle growth during the solid-state reaction. When increasing the carbon content from 2.1 to 7.3 wt%, the electrical DC conductivity of the composite measured from pressed pellets of the dry powder increases by three orders of magnitude. The thickness of the residual carbon coating on the olivine nanoparticles was determined from TEM measurements. Figure 3a and b shows TEM images of $LiFePO_4$/C with a residual carbon content of 7.3 wt% indicating that particles are homogenously coated by a layer with a thickness of about 3 nm.

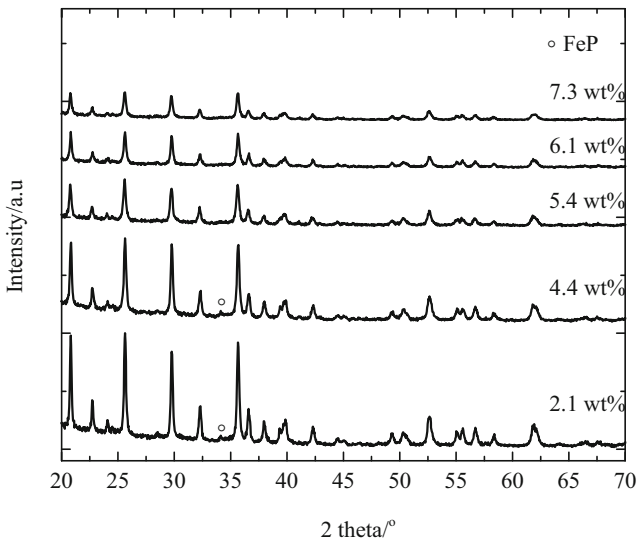

Fig. 2 XRD patterns of $LiFePO_4$/C produced with various amounts of glucose. While some traces of FeP (circles) appear at lower carbon content, phase pure materials could be synthesized from 5.4 wt% of carbon and above

Table 1 Physical properties of $LiFePO_4$/C with different carbon content after solid-state reaction at 700 °C

Sample	Amount of carbon (wt%)	Specific surface area (m^2/g)	Particle $size_{(BET)}$ (nm)	Crystallite size D_{XRD} (nm)	Conductivity (S/cm)
1	2.1	19	87	39	5.2×10^{-5}
2	4.4	35	47	34	3.5×10^{-4}
3	5.4	52	31	31	7.5×10^{-3}
4	6.1	56	29	36	1.0×10^{-2}
5	7.3	65	25	33	6.4×10^{-2}

This is in good agreement with the value calculated from the amount of carbon assuming spherical, monodisperse particles with homogeneous coating. The nature of the residual carbon was characterized with Raman spectroscopy. The spectra in Fig. 4 are dominated by two peaks related to disordered sp^2 carbon ("D", 1354 cm^{-1}) and graphitic sp^3 carbon ("G", 1597 cm^{-1}). Their relative contribution does not significantly depend on the carbon content. The result is comparable to the findings of Kadoma et al. [16] who calcined $LiFePO_4$/C between 600 and 800 °C. As the XRD patterns do not show any indication for crystalline carbon, it can be concluded that the carbon coating is mostly amorphous.

Based on the findings and results mentioned above, we decided to use 700 °C as the standard reaction temperature for solid-state synthesis of $LiFePO_4$/C. Under these conditions, the residual carbon content is sufficiently high for providing good conductivity and good crystallographic purity is reached.

Manganese addition

Figure 5 shows a comparison of the X-ray diffraction patterns for nanocomposite $LiFePO_4$/C and $LiFe_{0.7}Mn_{0.3}PO_4$/C. Both patterns indicate an identical, highly crystalline structure and can be matched to the orthorhombic olivine structure. Rietveld refinement revealed that the substitution of 30 mol% of iron by manganese yields an increase in the unit cell volume from 291.55 to 293.81 $Å^3$ (see Table 2) obeying Vegard's Law [29].

To keep the fraction of electrochemically-inactive carbon as low as possible while providing sufficient conductivity and small particles, a carbon content of 4–5 % was chosen for the investigation of manganese-containing lithium iron phosphate. Accordingly, $LiFe_{0.7}Mn_{0.3}PO_4$/C with 4.0 wt% of carbon was synthesized resulting in a mean particle size (calculated from BET measurements) of 54 nm. Its electrical conductivity was 2.7×10^{-3} S/cm, more than one order of magnitude higher than the value measured for $LiFePO_4$/C with 4.4 wt% of carbon (see Table 1). A similar result was observed by Molenda et al. who reported a higher electrical conductivity for $LiFe_{0.45}Mn_{0.55}PO_4$ compared to

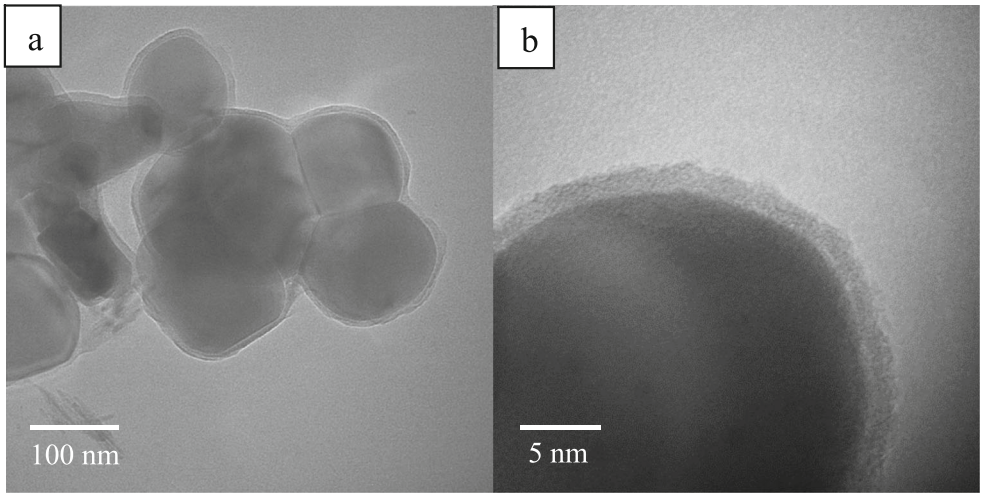

Fig. 3 TEM images of $LiFePO_4$/C containing 7.3 wt% of carbon

$LiFePO_4$ and attributed this observation to the presence of Fe^{2+}–Mn^{2+} pairs [27].

Electrochemical characterization

$LiFePO_4$/C

The electrochemical performance of $LiFePO_4$/C composites was investigated by cyclic voltammetry and constant-current charge/discharge measurements. Figure 6 shows the voltammograms of the first two cycles of $LiFePO_4$/C with various carbon contents.

Oxidation of Fe^{II} to Fe^{III} was detected at around 3.5 V versus Li/Li^+, and the corresponding reduction process occurs around 3.4 V according to Eq. 2:

$$Li\,Fe^{II}PO_4 \leftrightarrow Li_{1-x}\,Fe^{II}_{1-x}\,Fe^{III}_{x}PO + x\;Li^+ + x\;e^- \qquad (2)$$

The respective polarization of 107 to 160 mV is in consistence with literature [9, 12]. While an extremely broad oxidation peak was observed during the first cycle for the sample with 2.1 wt% carbon, the oxidation as well as the reduction peaks becomes sharper with increasing amount of carbon and the current maxima of the reduction process shift to higher values. This indicates that the increase in carbon content supports the current flow resulting in a higher discharge potential (cf. conductivities in Table 1). In addition, the decreasing particle size with increasing carbon content supports the ionic conductivity due to shorting of diffusion pathways for lithium ions. As usually observed, the peaks are sharper in the second cycle. This is attributed to limited diffusion during the first cycle and enhancement of wetting as well as modification of the electrode microstructure during the first cycle [12].

Figure 7 shows the discharge capacities of $LiFePO_4$/C recorded at 1 C for various carbon contents. Reversible capacities

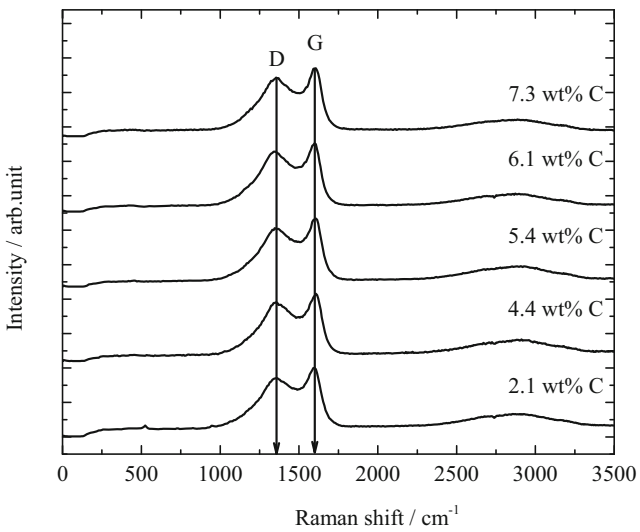

Fig. 4 Raman spectra of $LiFePO_4$/C with different amount of carbon. D: sp^2, G: sp^3 carbon

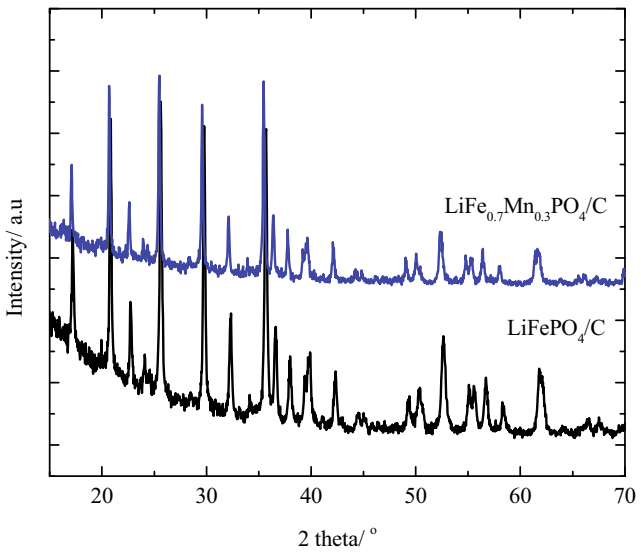

Fig. 5 X-ray diffraction pattern for nanocomposite $LiFePO_4$/C and $LiFe_{0.7}Mn_{0.3}PO_4$/C

Table 2 Lattice parameters of bare $LiFePO_4$/C and manganese doped $LiFe_{0.7}Mn_{0.3}PO_4$/C

Mn content/ mol%	Lattice parameters (Å)			Unit cell volume (Å^3)
	a	*b*	*c*	
0	10.328	6.011	4.696	291.55
30	10.355	6.026	4.709	293.81

between 77 and 114 mAh/g were observed with increasing carbon content and the discharge capacity for the sample with 2.1 wt% carbon slightly increased in time. We suggest an ongoing restructuring as the particle size of this material is comparably high and increasingly more particles became electrochemically active with time. The sample with 4.4 wt% carbon shows stable capacities over 75 cycles while a slight degradation was observed for the samples with 6.1 and 7.3 wt% carbon within the first 20 cycles. In comparison to the samples with minor carbon contents, unwanted side reactions with the electrolyte forming a passive layer may occur [3] due to their high-specific surface area that increasingly affects the electrochemical performance.

The average polarization potentials between charge and discharge processes at 1 C in dependence on the carbon content are depicted in Fig. 8. Due to the limited lithium-ion diffusion and the limited electronic conductivity, a polarization between the oxidation and reduction process occurs [6]. While the highest polarization was observed for the sample with 7.3 wt% carbon, the lowest polarization was found for materials with 2.08 and 4.36 wt% carbon.

This finding is related to the fact that the carbon layer on the particle surface noticeably hinders the lithium-ion diffusion with increasing thickness. Furthermore, the enlargement of the accessible particle surface with decreasing particle size raises the probability for side reactions with the electrolyte.

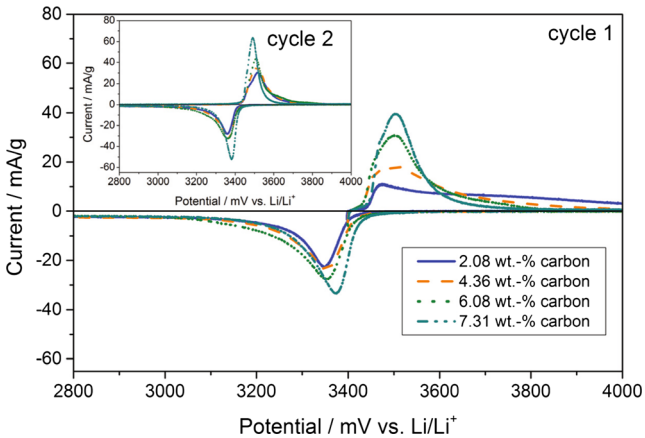

Fig. 6 Cyclic voltammogram of $LiFePO_4$/C composite electrodes with various carbon contents measured at a scan rate of 0.01 mV/s. The *inset* shows the corresponding cyclovoltammograms of the second cycle

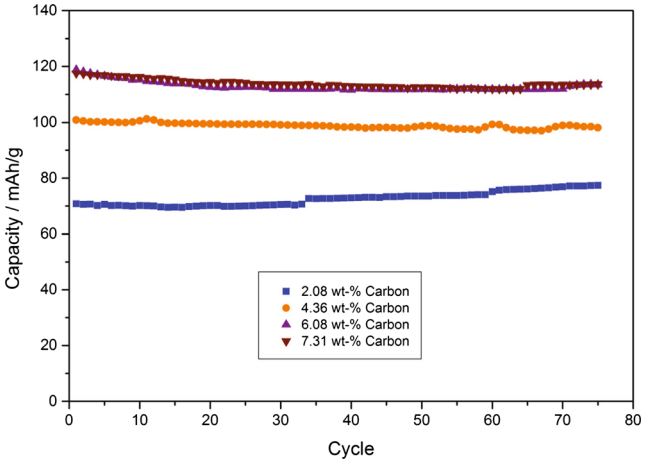

Fig. 7 Discharge capacities of $LiFePO_4$/C for various carbon contents with a charge/discharge rate of 1 C. The cut-off voltages were set to 2.6 and 4.2 V versus Li/Li$^+$

Herstedt et al. investigated the surface chemistry of carbon-coated $LiFePO_4$ and did not detect any solvent reaction products on cycled electrodes [14]. Therefore, it was suggested that the phosphate group did not participate in solvent reactions. Moreover, salt species consisting of $Li_xPF_yO_z$ were deposited on the particle surface. $Li_xPF_yO_z$ species can be formed by the hydrolysis of $LiPF_6$. Hence, we assume that quantitatively more salt species are deposited on the high-surface material, especially on the sample with 7.3 wt% of carbon (see Table 1). Accordingly, the highest polarization observed for the composite material with a carbon content of 7.3 wt% can be assigned to the limited lithium ion transfer through the carbon layer as well as to the presumably highest amount of passivation layer containing different salt decomposition products. Furthermore, the gradual reduction of the polarization potential in time can be attributed to slight

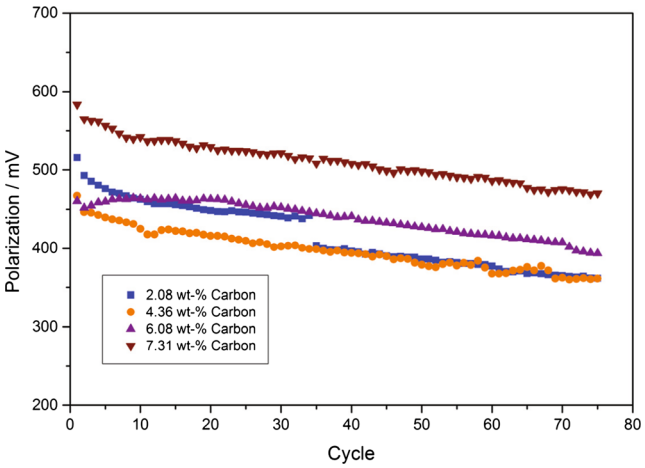

Fig. 8 Polarization between the charge and discharge processes of $LiFePO_4$/C depending on the carbon content in the active material with a charge/discharge rate of 1 C. The cut-off voltages were set to 2.6 and 4.2 V versus Li/Li$^+$

modifications of the electrode microstructure as well as to an enhanced wetting of the electrodes in time, thus resulting in facilitated lithium-ion transport.

Figure 9 shows the discharge capacities in dependence on the carbon content at different C rates. Due to ionic and electronic limitations, capacities decrease with increasing C rate for all materials. At C/20, discharge capacities between 102 and 146 mAh/g were obtained and dropped down to 46–69 mAh/g at 8 C. The lowest values were obtained for the sample with 2.1 wt% carbon while the measurements of the samples with 6.1 and 7.3 wt% carbon were very similar and showed the highest values. The discharge capacities at 16 C were in the 30–40 mAh/g range indicating that the difference between the samples narrows significantly. At this high discharge current, limitations might also occur from the lithium counter electrode and the electrolyte used which will be discussed later.

Our experiments show two main results: Firstly, the content of carbon in the active material has a crucial impact on the overall performance of $LiFePO_4$/C-based electrodes. By increasing the amount of carbon, the electrical conductivity of $LiFePO_4$/C can be enhanced by three orders of magnitude relative to the case with 2.1 wt% carbon (see Table 1). Nevertheless, increasing carbon contents also increase the mass of electrochemically inactive material. Secondly, by comparing the samples with 6.1 and 7.3 wt% carbon, it can be found that the discharge capacities (cf. Figs. 7 and 9) are almost identical. However, the high carbon content and the reduced particle size of the sample with 7.3 wt% carbon lead to a higher polarization, cf. Fig. 8. Decomposition products from the electrolyte at the surface of the active material as well as the carbon layer hinder the transport of lithium ions and electrons during the intercalation process of lithium into the host matrix.

An additional charge- and discharge-rate-limiting effect was found related to the ionic conductivity of the electrolyte.

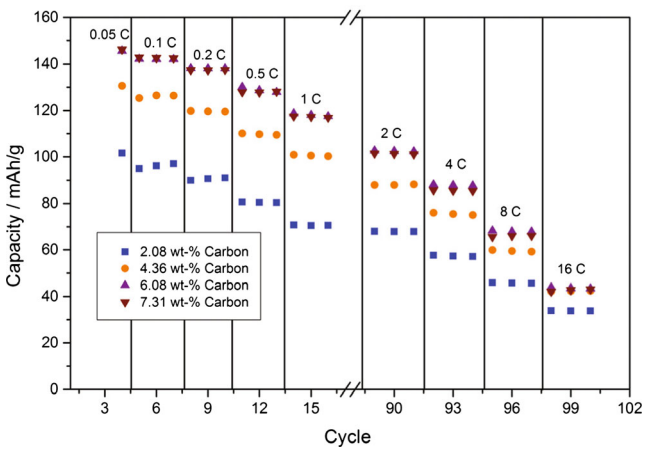

Fig. 9 Discharge capacities of $LiFePO_4$/C in dependence on the carbon content measured at different discharge rates

Due to its electrochemical stability at higher voltages (required for the measurement of manganese-containing material), the common electrolyte EC/DEC was replaced by EC/DMC. By comparing the capacity of the sample with 4.4 wt% of carbon at 16 C using a solution of EC/DMC instead of EC/DEC, a rise in capacity from 42 to 62 mAh/g was observed (compare Figs. 9 and 12). We attribute this to the higher ionic conductivity as well as higher electrochemical stability of EC/DMC compared to EC/DEC.

$LiFe_{0.7}Mn_{0.3}PO_4$/C

As shown before (see Fig. 7), the $LiFePO_4$/C composite material with a carbon content of 4.4 wt% shows a very stable electrochemical performance without any significant restructuring or degradation. Therefore, manganese-containing iron phosphate with a similar carbon content (4 wt%) was prepared and chosen for a comparative study, and the electrolyte system was changed from $LiPF_6$/EC/DEC to $LiPF_6$/EC/DMC due to better electrochemical stability of the latter one at higher voltages.

The electrochemically active incorporation of manganese is shown in Fig. 10. The cyclic voltammograms of $LiFePO_4$/C and $LiFe_{0.7}Mn_{0.3}PO_4$/C show that besides the oxidation of iron at about 3.5 V an additional oxidation step at around 4.05 V related to manganese can be observed. The reduction of manganese occurs at a potential of 3.91 V while the reduction potential of iron in the manganese-containing sample is observed at 3.41 V. This value is slightly shifted compared to 3.36 V observed for $LiFePO_4$/C which is in accordance with literature data [18] and can be explained by widening of the olivine-type unit cell through substitution of iron by manganese (see lattice values listed in Table 2). The results indicate that the reduction of the polarization between oxidation and reduction reaction of Fe^{II}/Fe^{III} originates from the substitutional embedding of manganese. It mainly affects the discharge rather than

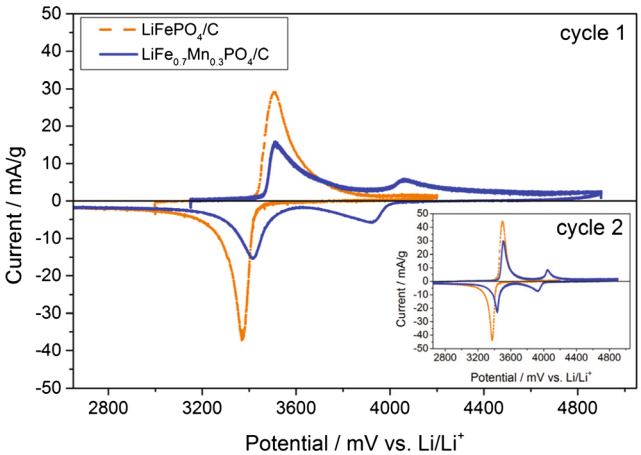

Fig. 10 Cyclic voltammograms of $LiFePO_4$/C and $LiFe_{0.7}Mn_{0.3}PO_4$/C composite electrodes measured at a scan rate of 0.01 mV/s. The inset shows the corresponding cyclic voltammograms of the second cycle

the charge reaction. This finding is consistent with the results of Nakamura et al. [29] who observed that the oxidation process in olivines is faster than the reduction process. In addition, they attribute the lower polarization by manganese addition to faster lithium ion diffusion. Besides the enhancement of the ionic conductivity, the electrical conductivity of $LiFePO_4$ is also increased by manganese addition [29].

Figure 11 illustrates the discharge capacities at a charge/discharge rate of 1 C of $LiFePO_4$/C and $LiFe_{0.7}Mn_{0.3}PO_4$/C with carbon contents in the range of 4 wt%. Discharge capacities of 102 mAh/g for $LiFePO_4$/C (carbon content 4.4 wt%) and 104 mAh/g for the $LiFe_{0.7}Mn_{0.3}PO_4$/C composite material were obtained. In the manganese-containing material, the discharge capacity slightly increases by about 2 mAh/g. Despite a higher cut-off potential compared to $LiFePO_4$/C, no capacity drop within the first cycles was observed. However, in contrast to $LiFePO_4$/C, the efficiency within the first cycle at C/20 for the manganese-containing material was less than 90 % indicating the formation of a passive layer during the first cycle.

Figure 12 shows the discharge capacities of $LiFePO_4$/C and $LiFe_{0.7}Mn_{0.3}PO_4$/C as a function of the discharge rate. The capacities were almost identical over the whole range of discharge rates with slightly higher values found for the manganese-containing samples. A similar trend was found by Lee et al. [32]. Lin et al. [24] observed an increased capacity of $LiFePO_4$ doped with 2 mol% Mn while Yoncheva et al. obtained a capacity decrease of $LiFePO_4$ with 50 mol% Mn [36]. It is apparent that the manganese concentration has a crucial impact on the electrochemical performance due to the influences of structure stabilities, lithium ion diffusion coefficients, and electrical conductivity. Compared to the electrolyte system based on EC/DEC (cf. Fig. 9), the measurements shown here clearly indicate that the better ionic conductivity of EC/DMC results in higher discharge rates from 8 C and above.

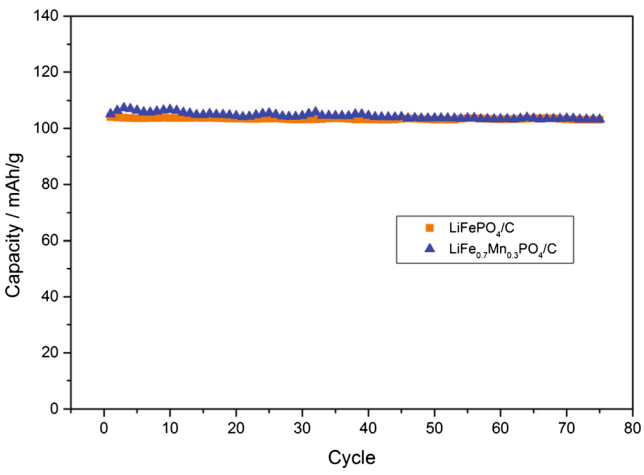

Fig. 11 Discharge capacities of $LiFePO_4$/C and $LiFe_{0.7}Mn_{0.3}PO_4$/C with a charge/discharge rate of 1 C. The cut-off voltages for $LiFePO_4$/C were set to 2.6 and 4.2 V versus Li/Li^+ and for the manganese-containing sample to 2.6 and 4.7 V versus Li/Li^+

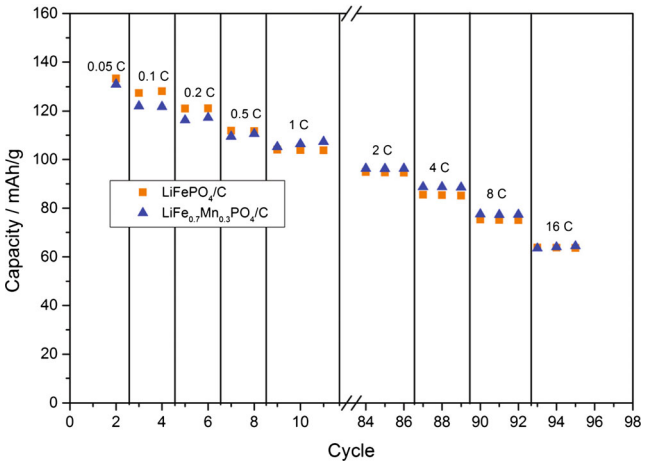

Fig. 12 Discharge capacities of $LiFePO_4$/C and $LiFe_{0.7}Mn_{0.3}PO_4$/C at various charge/discharge rates. From discharge rates between 1 C and 16 C, the charge rate was set to 1 C. The cut-off voltages for $LiFePO_4$/C and $LiFe_{0.7}Mn_{0.3}PO_4$/C were 2.6/4.2 V and 2.6/4.7 V versus Li/Li^+, respectively

Figure 13 shows the discharge curves for $LiFePO_4$/C and $LiFe_{0.7}Mn_{0.3}PO_4$/C at C rates of C/20 and 4 C. From the discharge curves at 0.05 C, the ratio between manganese and iron was estimated. The reduction of manganese showed a discharge capacity of about 40 mAh/g and the reduction of iron approximately 90 mAh/g which results in an iron/manganese ratio of 2.3:1.0. Thus, the chemical composition of lithium iron manganese phosphate containing 30 % of manganese could be confirmed by the electrochemical measurements. It is obvious from the graphs shown in Fig. 13 that the energy density of the material is increased by manganese doping as expected from the higher redox potential of Mn^{2+}/Mn^{3+} compared to Fe^{2+}/Fe^{3+}. In case of the measurements performed at 4 C, an increase from 273 to 295 mWh/g was found.

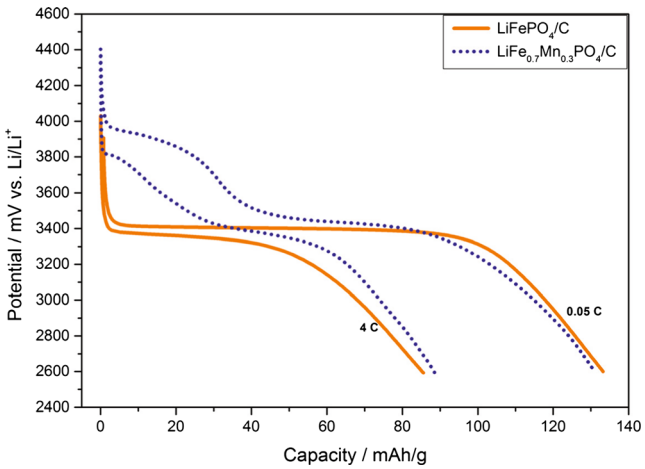

Fig. 13 Discharge curves of $LiFePO_4$/C (*solid line*) and $LiFe_{0.7}Mn_{0.3}PO_4$/C (*dashed line*) at 0.05 C and 4 C

Conclusions

A combined gas-phase/solid-state reaction method was used to synthesize high-purity nanosized $LiFePO_4$/C and the influence of carbon content and manganese addition on the materials' properties was investigated. A solid-state reaction temperature of 700 °C was found to create an almost phase pure $LiFePO_4$/C with olivine structure. While the crystallite size slightly decreases with increasing amount of carbon, the specific surface area as measured by BET was significantly affected. This is attributed to the fact that the increasing amount of carbon efficiently prevents the olivine nanoparticles from sintering. In parallel, the electronic conductivity of the $LiFePO_4$/C composites substantially increased by three orders of magnitude by increasing the amount of carbon from 2.1 to 7.3 wt%. Materials with the highest carbon content also showed the highest rate capabilities at all C rates measured. It was found, however, that the increased specific surface area in combination with the respective carbon content leads to a rising polarization potential between charge and discharge processes. Taking into account all properties required for good performance materials, a carbon content around 4 wt% provides the best compromise. The influence of a partial (30 mol%) exchange of iron by manganese was investigated by adding the respective manganese precursor to the mixture prepared for spray-flame synthesis. A successful integration of manganese could be shown by measuring the electrochemical properties. Due to an increase in lattice constants of the doped material a slight shift in the redox potential of Fe^{2+}/Fe^{3+} in combination with increased conductivity was found. Moreover, the energy density of $LiFePO_4$/C could be significantly enhanced by manganese addition.

Acknowledgments Financial support by the European Union and the Ministry of Innovation, Science and Research of the State of North Rhine-Westphalia in Germany (NanoEnergieTechnikZentrum, NETZ, Objective 2 Program: European Regional Development Fund, ERDF) is gratefully acknowledged. N.A. Hamid is thankful for financial support by the Government of Malaysia. The authors thank H. Grimm for help with TEM characterization and Günther Prinz for Raman spectroscopy.

References

1. Adams S (2010) Lithium ion pathways in $LiFePO_4$ and related olivines. J Solid State Electrochem 14(10):1787–1792
2. Belharouak I, Lu W, Vissers D, Amine K (2006) Safety characteristics of $Li(Ni_{0.8}Co_{0.15}Al_{0.05})O_2$ and $Li(Ni_{1/3}Co_{1/3}Mn_{1/3})O_2$. Electrochem Commun 8(2):329–335. doi:10.1016/j.elecom.2005.12.007
3. Cai ZP, Liang Y, Li WS, Xing LD, Liao YH (2009) Preparation and performances of $LiFePO_4$ cathode in aqueous solvent with polyacrylic acid as a binder. J Power Sources 189(1):547–551. doi:10.1016/j.jpowsour.2008.10.040
4. Chen Z-y, Zhu H-l, Ji S, Fakir R, Linkov V (2008) Influence of carbon sources on electrochemical performances of LiFePO4/C composites. Solid State Ionics 179(27–32):1810–1815. doi:10.1016/j.ssi.2008.04.018
5. Cheng F, Wan W, Tan Z, Huang Y, Zhou H, Chen J, Zhang X High power performance of nano-$LiFePO_4$/C cathode material synthesized via lauric acid-assisted solid-state reaction. Electrochimica Acta In Press, Corrected Proof. doi:10.1016/j.electacta.2011.01.007
6. Chung S-Y, Bloking JT, Chiang Y-M (2002) Electronically conductive phospho-olivines as lithium storage electrodes. Nat Mater 1(2):123–128
7. Delmas C, Cherkaoui F, Nadiri A, Hagenmuller P (1987) A nasicon-type phase as intercalation electrode: $NaTi_2(PO_4)_3$. Mater Res Bull 22(5):631–639. doi:10.1016/0025-5408(87)90112-7
8. Ellis BL, Wagemaker M, Mulder FM, Nazar LF (2010) Comment on "Aliovalent Substitutions in Olivine Lithium Iron Phosphate and Impact on Structure and Properties". Adv Funct Mater 20(2):186–188. doi:10.1002/adfm.200900673
9. Fedorková A, Oriňáková R, Oriňák A, Wiemhöfer H-D, Kaniansky D, Winter M (2010) Surface treatment of $LiFePO_4$ cathode material with PPy/PEG conductive layer. J Solid State Electrochem 14(12):2173–2178. doi:10.1007/s10008-009-0967-2
10. Gao F, Tang Z, Xue J (2007) Preparation and characterization of nano-particle $LiFePO_4$ and $LiFePO_4$/C by spray-drying and post-annealing method. Electrochim Acta 53(4):1939–1944. doi:10.1016/j.electacta.2007.08.048
11. Gao F, Tang Z, Xue J (2008) Effects of different iron sources on the performance of $LiFePO_4$/C composite cathode materials. J Univ Sci Technol Beijing Miner Metall Mater 15(6):802–807. doi:10.1016/s1005-8850(08)60291-1
12. Hamid NA, Wennig S, Hardt S, Heinzel A, Schulz C, Wiggers H (2012) High-capacity cathodes for lithium-ion batteries from nanostructured $LiFePO_4$ synthesized by highly-flexible and scalable flame spray pyrolysis. J Power Sources 216:76–83. doi:10.1016/j.jpowsour.2012.05.047
13. Hartner S, Ali M, Schulz C, Winterer M, Wiggers H (2009) Electrical properties of aluminum-doped zinc oxide (AZO) nanoparticles synthesized by chemical vapor synthesis. Nanotechnology 20(44):445701. doi:10.1088/0957-4484/20/44/445701
14. Herstedt M, Stjerndahl M, Nyten A, Gustafsson T, Rensmo H, Siegbahn H, Ravet N, Armand M, Thomas JO, Edstrom K (2003) Surface chemistry of carbon-treated LiFePO4 particles for Li-ion battery cathodes studied by PES. Electrochem Solid State Lett 6(9):A202–A206. doi:10.1149/1.1594413
15. Julien CM, Mauger A, Zaghib K (2011) Surface effects on electrochemical properties of nano-sized $LiFePO_4$. J Mater Chem 21(27):9955–9968
16. Kadoma Y, Kim J-M, Abiko K, Ohtsuki K, Ui K, Kumagai N (2010) Optimization of electrochemical properties of $LiFePO_4$/C prepared by an aqueous solution method using sucrose. Electrochim Acta 55(3):1034–1041. doi:10.1016/j.electacta.2009.09.029
17. Kim J-K, Choi J-W, Chauhan GS, Ahn J-H, Hwang G-C, Choi J-B, Ahn H-J (2008) Enhancement of electrochemical performance of lithium iron phosphate by controlled sol-gel synthesis. Electrochim Acta 53(28):8258–8264. doi:10.1016/j.electacta.2008.06.049
18. Kobayashi G, Yamada A, S-i N, Kanno R, Kobayashi Y, Seki S, Ohno Y, Miyashiro H (2009) Shift of redox potential and kinetics in $Li_x(Mn_yFe_{1-y})PO_4$. J Power Sources 189(1):397–401. doi:10.1016/j.jpowsour.2008.07.085
19. Konarova M, Taniguchi I (2009) Physical and electrochemical properties of $LiFePO_4$ nanoparticles synthesized by a combination of spray pyrolysis with wet ball-milling. J Power Sources 194(2):1029–1035. doi:10.1016/j.jpowsour.2009.06.046
20. Kosova NV, Devyatkina ET, Petrov SA (2010) Fast and Low Cost Synthesis of LiFePO4 Using Fe3+ Precursor. J Electrochem Soc 157(11):A1247–A1252. doi:10.1149/1.3489292
21. Kulka A, Baster D, Dudek M, Kielbasa M, Milewska A, Zajac W, Swierczek K, Molenda J (2013) Electrochemical properties of

chemically modified phosphoolivines as cathode materials for Li-ion batteries. J Power Sources 244:565–569. doi:10.1016/j.jpowsour.2013.01.156
22. Li C, Hua N, Wang C, Kang X, Tuerdi W, Han Y (2011) Effect of Mn^{2+}-doping in $LiFePO_4$ and the low temperature electrochemical performances. J Alloys Compd 509(5):1897–1900. doi:10.1016/j.jallcom.2010.10.083
23. Lin Y, Gao MX, Zhu D, Liu YF, Pan HG (2008) Effects of carbon coating and iron phosphides on the electrochemical properties of $LiFePO_4$/C. J Power Sources 184(2):444–448. doi:10.1016/j.jpowsour.2008.03.026
24. Lin Y, Zeng B, Lin Y, Li X, Zhao G, Zhou T, Lai H, Huang Z (2012) Electrochemical properties of carbon-coated $LiFePO_4$ and $LiFe_{0.98}Mn_{0.02}PO_4$ cathode materials synthesized by solid-state reaction. Rare Metals 31(2):145–149. doi:10.1007/s12598-012-0480-0
25. Lutterotti L, Matthies S, Wenk HR (1999) MAUD: A friendly Java program for material analysis using diffraction. ICUr: Newsletter of the CPD, p 14
26. Mi CH, Zhang XG, Zhao XB, Li HL (2006) Effect of sintering time on the physical and electrochemical properties of $LiFePO_4$/C composite cathodes. J Alloys Compd 424(1–2):327–333. doi:10.1016/j.jallcom.2005.12.062
27. Molenda J, Qjczyk W, Marzec J (2007) Electrical conductivity and reaction with lithium of $LiFe_{1-y}Mn_yPO_4$ olivine-type cathode materials. J Power Sources 174(2):689–694. doi:10.1016/j.jpowsour.2007.06.238
28. Mueller R, Madler L, Pratsinis SE (2003) Nanoparticle synthesis at high production rates by flame spray pyrolysis. Chem Eng Sci 58(10):1969–1976. doi:10.1016/s0009-2509(03)00022-8
29. Nakamura T, Sakumoto K, Okamoto M, Seki S, Kobayashi Y, Takeuchi T, Tabuchi M, Yamada Y (2007) Electrochemical study on Mn^{2+}-substitution in $LiFePO_4$ olivine compound. J Power Sources 174(2):435–441. doi:10.1016/j.jpowsour.2007.06.191
30. Rellinghaus B, Lindackers D, Kockerling M, Roth P, Wassermann EF (2003) The process of particle formation in the flame synthesis of tin oxide nanoparticles. Phase Transit 76(4–5):347–354. doi:10.1080/0141159021000051442
31. Wang J, Sun X (2012) Understanding and recent development of carbon coating on $LiFePO_4$ cathode materials for lithium-ion batteries. Energy Environ Sci 5(1):5163–5185
32. Wang DY, Li H, Shi SQ, Huang XJ, Chen LQ (2005) Improving the rate performance of $LiFePO_4$ by Fe-site doping. Electrochim Acta 50(14):2955–2958. doi:10.1016/j.electacta.2004.11.045
33. Wang Y, Wang Y, Hosono E, Wang K, Zhou H (2008) The design of a $LiFePO_4$/carbon nanocomposite with a core–shell structure and its synthesis by an in situ polymerization restriction method. Angew Chem Int Ed 47(39):7461–7465. doi:10.1002/anie.200802539
34. Wang Y, Zhang D, Yu X, Cai R, Shao Z, Liao X-Z, Ma Z-F (2010) Mechanoactivation-assisted synthesis and electrochemical characterization of manganese lightly doped $LiFePO_4$. J Alloys Compd 492(1–2):675–680. doi:10.1016/j.jallcom.2009.12.014
35. Xia Y, Yoshio M, Noguchi H (2006) Improved electrochemical performance of $LiFePO_4$ by increasing its specific surface area. Electrochim Acta 52(1):240–245. doi:10.1016/j.electacta.2006.05.002
36. Yoncheva M, Koleva V, Mladenov M, Sendova-Vassileva M, Nikolaeva-Dimitrova M, Stoyanova R, Zhecheva E (2011) Carbon-coated nano-sized $LiFe_{1-x}Mn_xPO_4$ solid solutions ($0 \le x \le 1$) obtained from phosphate–formate precursors. J Mater Sci 46(22):7082–7089. doi:10.1007/s10853-011-5555-z
37. Zhang L, Xiang H, Zhu X, Yang W, Wang H (2012) Synthesis of $LiFePO_4$/C composite as a cathode material for lithium-ion battery by a novel two-step method. J Mater Sci 47(7):3076–3081. doi:10.1007/s10853-011-6139-7